The EMBO Journal Vol.18 No.13 pp.3533–3545, 1999

Crystal structures of adenine phosphoribosyltransferase from *Leishmania donovani*

Cynthia L.Phillips[1], Buddy Ullman[2], Richard G.Brennan[2] and Christopher P.Hill

Biochemistry Department, University of Utah, Salt Lake City, UT 84132 and [2]Department of Biochemistry and Molecular Biology, L-224, Oregon Health Sciences University, Portland, OR 97201, USA

[1]Corresponding author
e-mail: cynthia@snowbird.med.utah.edu

The enzyme adenine phosphoribosyltransferase (APRT) functions to salvage adenine by converting it to adenosine-5-monophosphate (AMP). APRT deficiency in humans is a well characterized inborn error of metabolism, and APRT may contribute to the indispensable nutritional role of purine salvage in protozoan parasites, all of which lack *de novo* purine biosynthesis. We determined crystal structures for APRT from *Leishmania donovani* in complex with the substrate adenine, the product AMP, and sulfate and citrate ions that appear to mimic the binding of phosphate moieties. Overall, these structures are very similar to each other, although the adenine and AMP complexes show different patterns of hydrogen-bonding to the base, and the active site pocket opens slightly to accommodate the larger AMP ligand. Whereas AMP adopts a single conformation, adenine binds in two mutually exclusive orientations: one orientation providing adenine-specific hydrogen bonds and the other apparently positioning adenine for the enzymatic reaction. The core of APRT is similar to that of other phosphoribosyltransferases, although the adenine-binding domain is quite different. A C-terminal extension, unique to *Leishmania* APRTs, extends an extensive dimer interface by wrapping around the partner molecule. The active site involves residues from both subunits of the dimer, indicating that dimerization is essential for catalysis.

Keywords: adenine phosphoribosyltransferase/crystal structure/*Leishmania donovani*/purines

Introduction

In mammals and other organisms that can synthesize purines *de novo*, recycling of purines is important primarily during periods of rapid growth, such as embryogenesis and tumor proliferation (Weber *et al.*, 1987; Pillwein *et al.*, 1990). The ubiquitous enzyme adenine phosphoribosyltransferase (APRT) specifically salvages adenine by catalyzing its conversion to adenosine-5-monophosphate (AMP) (Figure 1). Although APRT defects are not lethal in humans, they do cause 2,8-dihydroxyadenine urolithiasis (a rare form of kidney stones) (Musick, 1981; Simmonds *et al.*, 1995). In contrast, protozoan parasites lack a *de novo* biosynthetic pathway for purines and must therefore scavenge purines from their host (Berens *et al.*, 1995). Likewise, the importance of purine recycling for tumor cells relative to normal human cells points to APRT and other enzymes of the purine salvage pathway as potential targets for chemotherapeutic intervention.

The parasite *Leishmania donovani* causes visceral leishmaniasis, which is a fatal disease if untreated. Unfortunately, the treatments currently available involve highly toxic and non-selective drugs. Although APRT is not essential for purine salvage in *L.donovani* promastigotes (Hwang and Ullman, 1997), the form that lives in the sandfly vector, APRT may play an essential role in the infective amastigote form of the parasite that lives in the host macrophage cells (Looker *et al.*, 1983). Thus, the parasite APRT is a target for anti-leishmanial chemotherapy.

Leishmania donovani APRT belongs to the family of type I phosphoribosyltransferases (PRTs) for which several three-dimensional structures are known (Table I). PRT structures share a common core region of at least five parallel β-strands surrounded by three or more helices. The core includes a 13-residue sequence known as the α-D-5-phosphoribosyl-1-pyrophosphate (PRPP)-binding motif (Argos *et al.*, 1983; Hershey and Taylor, 1986; Hove-Jensen *et al.*, 1986) that binds the ribose ring and 5′-phosphate of PRPP in crystal structures of enzyme complexes with substrate or product. A flexible loop within the core sequence appears to provide a shielded environment at the active site during catalysis (Scapin *et al.*, 1995; Schumacher *et al.*, 1996; Krahn *et al.*, 1997; Focia *et al.*, 1998a; Wang *et al.*, 1999b). Type I PRTs also have a structurally variable region, known as the 'hood', which is responsible primarily for base recognition and the definition of substrate specificity.

Type I PRTs have been shown to bind PRPP followed by the ribose-5-phosphate acceptor (adenine in the case of APRT) (Bhatia *et al.*, 1990; Yuan *et al.*, 1992; Wang *et al.*, 1999a). Nucleophilic attack at the PRPP ribose C1′, which proceeds with inversion of stereochemistry, has been proposed to follow either SN1 or SN2 displacements. In an SN1 reaction, which is favored in the case of the OPRTs (Scapin *et al.*, 1995), an oxocarbonium intermediate would be formed before the adenine N_9 attacks the ribose C1′. This positively charged intermediate would require protection from solvent to prevent hydrolysis. For an SN2 reaction, as is favored in the case of *Trypanosoma cruzi* HGPRT (Focia *et al.*, 1998b), the enzyme would promote simultaneous nucleophilic attack and product formation.

Type I PRTs require a divalent metal ion, typically Mg^{2+} or Mn^{2+}, for activity. Most type I PRT crystal structures have identified a Mg^{2+} or Mn^{2+} coordinated to conserved acidic residues of the PRPP-binding motif (Scapin *et al.*, 1995; Schumacher *et al.*, 1996; Vos *et al.*,

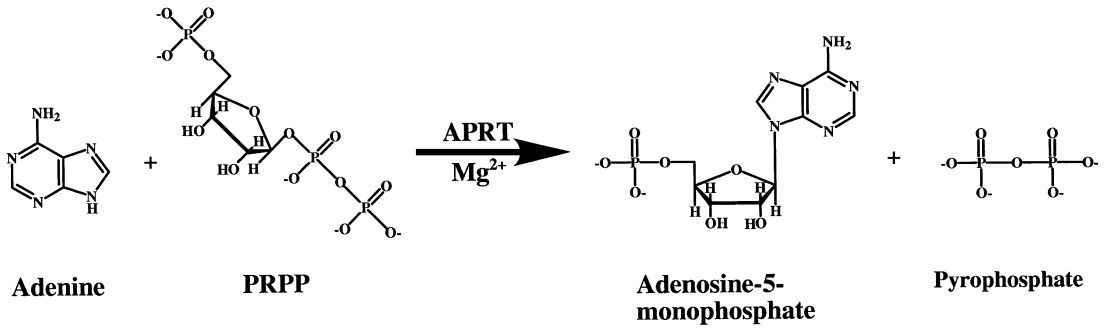

Fig. 1. Reaction catalyzed by APRT. A phosphoribosyl group is transferred from PRPP to the N_9 nitrogen of adenine in the presence of magnesium, forming adenosine-5′-monophosphate and pyrophosphate. Figures 1 and 7 were made using the program ChemDraw (CambridgeSoft Corp., Cambridge, MA).

Table I. Structures of phosphoribosyltransferases

PRT name	Abbreviation	Organism	Reference
Adenine PRT	APRT	*Leishmania donovani*	this paper
Uracil PRT	UPRT	*Toxoplasma gondii*	Schumacher *et al.* (1998)
Xanthine PRT	XPRT	*Escherichia coli*	Vos *et al.* (1997)
Orotate PRT	OPRT	*E.coli*	Henriksen *et al.* (1996)
Orotate PRT	OPRT	*Salmonella typhimurium*	Scapin *et al.* (1994, 1995)
Hypoxanthine-guanine PRT	HGPRT	*Trypanosoma cruzi*	Focia *et al.* (1998a,b)
Hypoxanthine-guanine PRT	HGPRT	*Homo sapiens*	Eads *et al.* (1994)
Hypoxanthine-guanine-xanthine PRT	HGXPRT	*Tritrichomonas foetus*	Somoza *et al.* (1996)
Hypoxanthine-guanine-xanthine PRT	HGXPRT	*T.gondii*	Schumacher *et al.* (1996)
Glutamine PRPP amidotransferase	GAT	*S.typhimurium*	Smith *et al.* (1994)
Glutamine PRPP amidotransferase	GAT	*E.coli*	Krahn *et al.* (1997); Muchmore *et al.* (1998)

1997). In PRPP-bound PRT structures, the Mg^{2+} or Mn^{2+} coordinates the 2′- and 3′-hydroxyls of the PRPP ribose, as well as oxygen(s) of the PRPP β-phosphate (Scapin *et al.*, 1995; Krahn *et al.*, 1997; Focia *et al.*, 1998b). In addition, a Mn^{2+} ligand in the GAT–PRPP complex (Krahn *et al.*, 1997) is coordinated by a water molecule that also hydrogen bonds with a conserved *cis*-peptide backbone carbonyl. Although the metal ligands are not exactly the same in each PRT structure in which a metal ion has been modeled, this metal binding site is in approximately the same region of the active site in type I PRT crystal structures. A second magnesium ion is also seen in the structure of *T.cruzi* HGPRT complexed with PRPP and a hypoxanthine analog (Focia *et al.*, 1998b). Contacts to this ion are made by the PRPP, the protein and several water molecules, one of which also hydrogen bonds with the hypoxanthine analog N_3, suggesting a role for this metal ion in positioning the purine base for nucleophilic attack at the PRPP ribose C1′.

In an effort to understand further the basis for substrate selection and catalysis by APRT, we have determined the crystal structure of the enzyme from *L.donovani* in complexes with the substrate adenine, the product AMP and anions that mimic reactant phosphate moieties. The core region of APRT resembles that of other PRTs, although the adenine binding domain and a C-terminal extension that contributes to dimerization are unique. The APRT structure most closely resembles that of OPRT, suggesting that these enzymes share a common catalytic mechanism and constitute a subclass of type I PRTs. The *L.donovani* APRT structure also suggests how the structure of the considerably smaller human APRT may differ, thus guiding the design of structure-based inhibitors or subversive substrates (cytotoxic substrate analogs of adenine) targeted specifically to the *L.donovani* APRT.

Results and discussion

Structure determination

The crystal structure of *L.donovani* APRT, grown from a solution containing $(NH_4)_2SO_4$, was determined by the method of multiple isomorphous replacement using data collected at room temperature. This structure, apo-AS–APRT, was refined at 2.48 Å resolution to an *R*-factor of 17.6% (R_{free} 25.0%). Apo-AS–APRT was used as the starting model to refine the structures of three other essentially isomorphous APRT crystals grown from solutions with PEG 5000 MME as the precipitant: unliganded APRT (apo–APRT; 1.98 Å resolution; *R*-factor 18.7%; R_{free} 24.1%), APRT with bound adenine (Ade–APRT; 1.5 Å resolution; *R*-factor 20.0%; R_{free} 23.9%), and APRT bound to AMP (AMP–APRT; 2.0 Å resolution; *R*-factor 19.6%; R_{free} 26.3%). The use of PEG as precipitant in place of ammonium sulfate was necessary for the formation of adenine and AMP complexes. It also allowed application of low temperature methods, which provided a dramatic improvement in data quality. See Table II for data collection statistics and Table III for heavy atom parameters and statistics.

The N-terminal methionine lacks defined density in all of the APRT structures and has not been modeled. N-terminal sequence analysis of APRT crystals revealed that this residue is absent in approximately half of the crystallized protein. Residues 120–123 are disordered and have been omitted from all the structures, although some weak density is visible in apo–APRT, Ade–APRT, and

Table II. Data collection statistics

	Hg	Se	Apo-AS–APRT	Apo–APRT	Ade–APRT	AMP–APRT
Space group $P6_122$						
Unit cell parameters: a, c (Å)	64.0, 239.7	64.0, 240.4	64.0, 240.5	63.8, 236.6	63.7, 235.8	64.0, 235.9
Resolution (Å)	2.64–18.0	2.26–14.7	2.48–18.6	1.98–19.7	1.5–35.0	2.0–19.0
Number of observations	26 480	35 867	33 527	349 744	496 588	328 256
Number of unique reflections	9395	11 138	9680	19 055	33 949	17 882
Mosaicity (deg.) (refined valued)	NA[a]	NA[a]	NA[a]	0.41	0.43	1.00
Completeness of data (%)	99.0 (66.0)	99.0 (50.1)	87.2 (63.2)	91.5 (61.3)	72.8 (42.8)	87.9 (60.3)
$I/\sigma(I)$	13.9 (4.4)	9.8 (4.5)	10.0 (2.6)	32.5 (10.2)	39.7 (2.51)	20.8 (3.87)
R_{sym}[b] (%)	5.8 (10.5)	6.0 (14.9)	12.9[c] (14.3)	5.1 (12.4)	4.0 (28.0)	5.3 (17.5)

Values in parentheses refer to the highest resolution shell.
[a]Not available.
[b]$R_{sym} = \Sigma|I_i - \langle I \rangle|/\Sigma I_i$.
[c]Data for apo-AS–APRT was collected in three resolution ranges, each using a different crystal. The high R_{sym} reflects the merging of data from these crystals.

Table III. Heavy atom derivatives used in structure determination of APRT

Derivative	Site	*x*	*y*	*z*	occ	B	Phasing power	R_{Cullis}[a]	R_{Kraut}[b]	# reflections	d_{min} (Å)	FOM	R_{iso}[c]
Hg	Hg1	0.6016	0.2523	0.6523	0.969	26.3							
	Hg2	0.3166	0.0586	0.5574	0.889	27.4	2.14	0.44	0.093	8673	3.0	0.47	20.2
Se	Se1	0.6622	0.3365	0.0294	1.000	20.0							
	Se2	0.3339	0.0830	0.1595	0.876	20.0							
	Se3	0.3874	0.1285	0.0843	0.916	20.0							
	Se4	0.6384	0.2648	0.7098	0.962	20.0							
	Se5	0.5736	0.1646	0.1405	0.935	20.0	0.70	0.66	0.174	8827	3.0	0.22	16.6
Total										6243 phased	3.0	0.59	

[a]$R_{Cullis} = \Sigma||F_{PH} \pm F_P| - |F_H(calc)||/ \Sigma|F_{PH} \pm F_P|$.
[b]$R_{Kraut} = \Sigma||F_{PH}| - |F_P + F_H(calc)||/ \Sigma|F_{PH}|$.
[c]$R_{iso} = (\Sigma||F_{deriv}| - |F_{native}||)/\Sigma|F_{native}|$, (%, relative to apo-AS–APRT data).

Table IV. Refinement statistics

	apo-AS–APRT	apo–APRT	Ade–APRT	AMP–APRT
Resolution range (Å)	2.48–18.6	1.98–19.7	1.5–35.0	2.0–19.0
[a]R_{cryst} (%)	17.6	18.7	20.0	19.6
[b]R_{free} (%)	25.0	24.1	23.9	26.3
RMS deviations from ideal				
Bond length (Å)	0.007	0.006	0.006	0.007
Bond angle (deg.)	1.3	1.4	1.3	1.3
Dihedral angle (deg.)	24.9	24.7	24.5	24.5
Improper angle (deg.)	1.13	1.21	1.19	1.16
Number of H_2O molecules	146	215	215	181
Average B-factor, protein ($Å^2$)	31	23	26	23
Average B-factor, H_2O (Mg) ($Å^2$)	41	33 (16)	36 (25)	34 (42)
Average B-factor, adenine or AMP ($Å^2$)			36	37
Average B-factor, citrate or sulfate ($Å^2$)	38	23	24	56
Ramachandran plot statistics				
Residues in most favored regions (%)	88.9	90.5	93.1	93.0
Residues in additionally allowed regions (%)	11.1	9.5	6.9	7.0
Residues in disallowed regions (%)	0.0	0.0	0.0	0.0

All data were used without rejection based on the estimated standard deviations. A bulk solvent correction was applied for the final map and *R*-factor calculations. Stereochemical criteria were defined using PROCHECK (Laskowski *et al.*, 1993).
[a]$R_{cryst} = \Sigma(||F_{obs}| - |F_{calc}||)/ \Sigma|F_{obs}|$, crystallographic *R*-factor.
[b]R_{free} is the *R*-factor for a selected subset (10%) of the reflections which were not included in prior refinement calculations.

AMP–APRT. Apo-AS–APRT also lacks defined density for residue 119 and residues 236 and 237 at the C-terminus. The structures crystallized from PEG all reveal a citrate molecule (from the crystallization buffer) bound in the active site, as well as the added ligand in the Ade–APRT and AMP–APRT structures. A single magnesium ion was also found at the active site of the Ade–APRT and AMP–APRT structures. The apo-AS–APRT structure contains two sulfate ions; one in the same location as the phosphate moiety of AMP, the other in the same position as the citrate of crystals grown from PEG. Refinement statistics are given in Table IV.

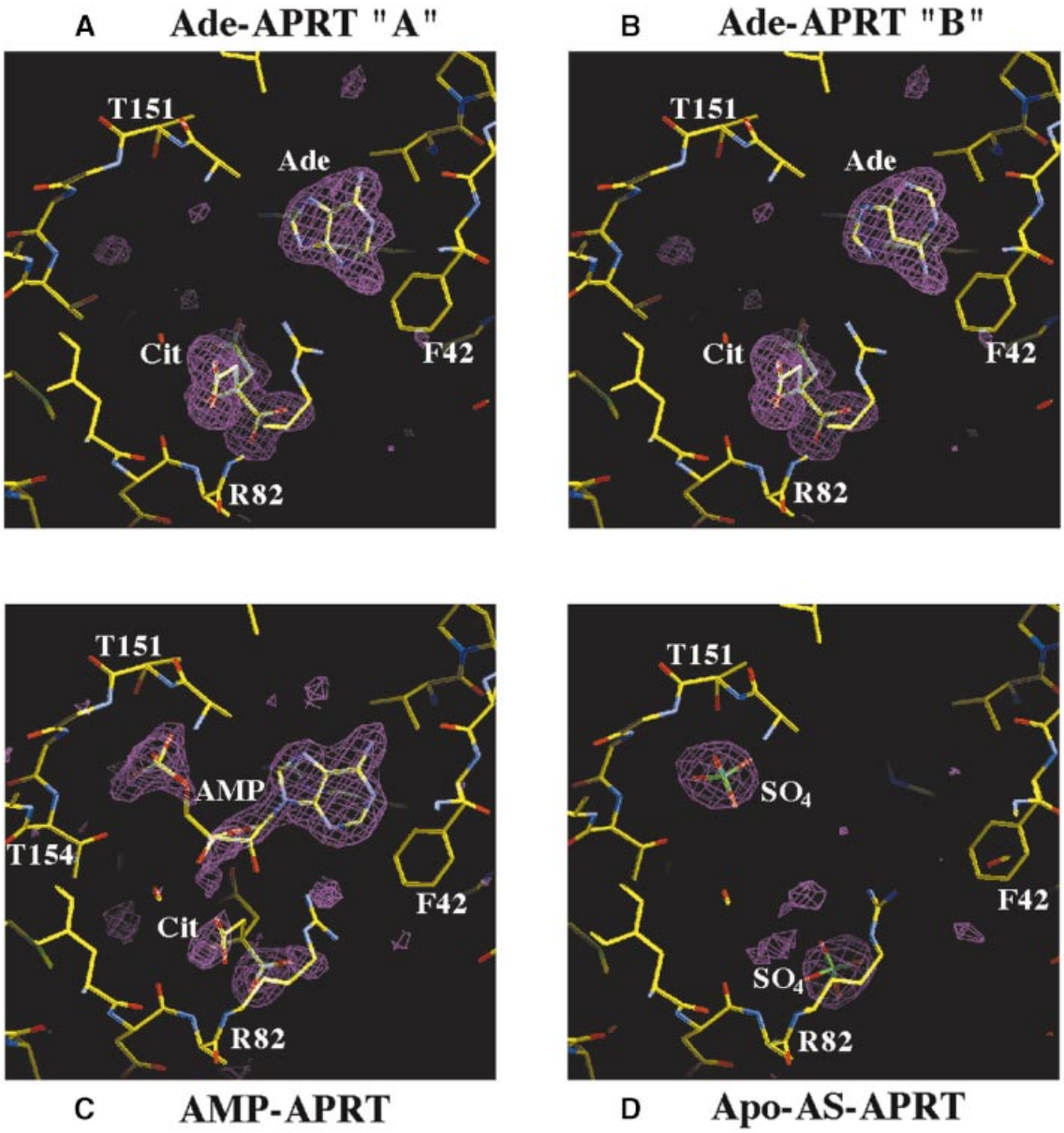

Fig. 2. Definition of ligands in electron density maps. F_o–F_c omit electron density maps, shown in violet at 3.0σ, were calculated after simulated annealing from 1000 K and 20 rounds of positional refinement in X-PLOR (Brünger, 1996). For clarity, the waters and magnesium ion are not shown. Refinement and phase calculations performed for: (**A**) the Ade–APRT model in which adenine (in orientation 'A') and citrate were omitted; (**B**) the Ade–APRT model in which adenine (in orientation 'B') and citrate were omitted; (**C**) the AMP–APRT model in which AMP and citrate were omitted; (**D**) the apo-AS–APRT model in which the two sulfates were omitted. These figures were made using the program O (Jones *et al.*, 1991).

The four structures determined are quite similar to each other. The highest resolution (1.5 Å) Ade–APRT model is used to describe general aspects of the APRT structure. Superposition of all C_α carbons of Ade–APRT onto those of either the apo–APRT or AMP–APRT structures results in an average r.m.s.d. of 0.24 Å, indicating that there are no gross structural changes upon adenine or AMP binding. In addition, superposition of the C_α carbons of apo–APRT and apo-AS–APRT structures also result in a low r.m.s.d. of 0.58 Å, indicating that neither freezing nor alternative (sulfate/citrate) anion coordination result in significant global structural changes in APRT. Electron density for the adenine, AMP, citrate and sulfate ligands is shown in Figure 2.

Monomer structure

The *L.donovani* APRT structure (Figure 3) includes nine β-strands (S1–S9) and 12 helices (H1–H12), and consists of four regions: the 'core', the 'flexible loop', the 'hood' and the C-terminal 'arm'. The APRT core, which is a conserved structure in type I PRTs, is comprised of a central β-sheet (strands S1, S2, S3, S4, S7, S8 and S9) that packs against helices H4 and H5 on one side and against H7 and H9 on the other side. The core includes a dinucleotide-binding fold, which provides the nucleotide-binding site near the C-terminal ends of the β-strands. The two β-α-β-α-β topologies of the APRT dinucleotide-binding fold are H4-S3-H5-S4 (which lacks one β-strand) and S7-H7-S8-H9-S9. As expected, the highly conserved

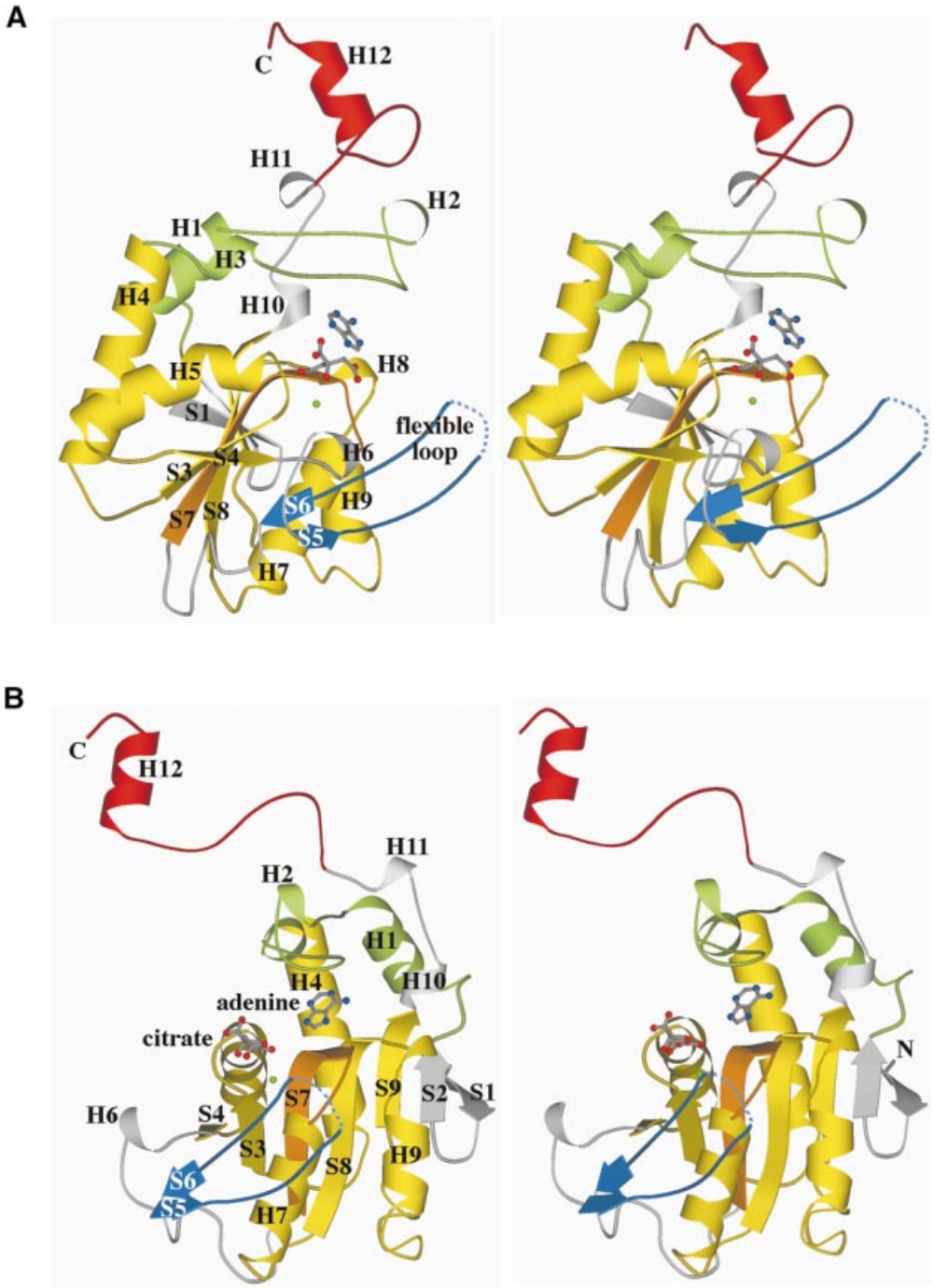

Fig. 3. Stereo ribbon diagram of monomer Ade–APRT. The PRT core is yellow, with residues 142–153 of the PRPP-binding motif in orange. The flexible loop is blue, with a dotted line at the tip indicating the position of the four residues (120–123) with poor electron density. The hood is green and the C-terminal arm is red. Secondary structural elements are labeled. Chain termini are indicated with an N or a C. The adenine and citrate are gray with the oxygen atoms red, and the nitrogen atoms blue. Adenine is shown in the 'A' orientation. The magnesium ion is green. View (**B**) is rotated 90° relative to view (**A**). Figures 3, 5, 8, 9 and 10 were made using the program MOLSCRIPT (Kraulis, 1991).

13-residue PRPP-binding motif, which is comprised of β-strand S7 and the following loop, adopts the same structure as seen in other type I PRTs (r.m.s.d. on C_α atoms is typically $<$1.0 Å). The flexible loop, which is located at one end of the β-sheet, tilts away from the core rather than extending the β-sheet as it does in other PRTs. Another feature distinguishing this APRT from other PRTs is seen at the opposite end of the core β-sheet, which in APRT is extended by the two N-terminal β-strands, S1 and S2.

The flexible loop of APRT and other type I PRTs originates in the middle of the PRT core sequence and is structurally positioned at one end of the core β-sheet. For most type I PRTs, this loop lies between the last β-strand of the dinucleotide-binding fold and an antiparallel β-strand that continues the twisted β-sheet of the core. In APRT, however, the last β-strand of the dinucleotide-binding fold (S4) is followed by a short helix (H6) and a β-ladder (S5 and S6) with the flexible loop contained between S5 and S6 and tilted away from the core (Figure 3).

The flexible loop apparently adopts an open conformation to allow substrate binding and a closed conformation during catalysis (Scapin *et al.*, 1994; Schumacher *et al.*, 1996; Wang *et al.*, 1999b). Indeed, structures of type I PRTs with bound PRPP reveal the loop in a closed conformation (Krahn *et al.*, 1997; Focia *et al.*, 1998b), whereas in most PRT structures PRPP is not bound, and the entire flexible loop is disordered. In contrast, all four of the APRT structures lack bound PRPP, yet show this loop in a conformation that is both open and ordered, with only the very tip of the loop (residues 120–123) lacking defined density. This open and ordered conformation of the APRT loop may be defined by an interaction between the tip of the loop and Ser70 of a symmetry-related molecule in the crystal lattice. Another possibility, that the closed conformation requires contacts to the substrate PRPP molecule, is supported by the observations that addition of PRPP slows proteolysis of the flexible loop in XPRT, and that removal of XPRT loop residues results in loss of catalytic activity without abrogating the ability to bind the product GMP (Vos *et al.*, 1997). The APRT loop structure may more closely resemble that observed for other PRT structures if it adopts a closed conformation during catalysis. In the open conformation, however, the loop is much further from the core β-sheet than is seen in open conformations of other type I PRTs.

The active site of type I PRTs is located between the PRT core and a structurally variable region called the 'hood' (Scapin *et al.*, 1994; Schumacher *et al.*, 1996, 1998) that provides most of the contacts to the nucleotide base and is thus primarily responsible for the base specificity of the various PRTs. The hood of APRT is composed of helices H1, H2, H3 and the N-terminus of H4, with most of the contacts to adenine made by the loop between helices H2 and H3. The APRT hood structure does not resemble that of any other known type I PRT and bears little resemblance to a model predicted for Chinese hamster APRT (de Boer and Glickman, 1991). Absent from the APRT hood is a contact to the adenine N_3 that is observed in all other purine/pyrimidine-binding type I PRTs and has been proposed to promote SN2-type nucleophilic attack (Focia *et al.*, 1998b).

The C-terminal 'arm' of *L.donovani* APRT is also a unique sub-structure distinct from that of other PRTs. Following the short helices H10 and H11, which project away from the core, the arm (residues 215–237) is formed by a loop and helix H12 that protrude from the monomer. Comparison of amino acid sequences indicate that this arm is unique to APRTs from *Leishmania* (Figure 4). As discussed below, the arm wraps around the partner molecule in the APRT dimer.

The APRT dimer

APRT forms an extensive dimer interface about a crystallographic two-fold axis (Figure 5A) that buries 2670 Å^2 of the total 13 290 Å^2 solvent-accessible surface area on each monomer (Hubbard and Thornton, 1993). Analysis by equilibrium centrifugation confirms that *L.donovani* APRT is a dimer in solution at pH 6.5 (Figure 6). This is in contrast to a previous gel filtration study that reported *L.donovani* APRT to be monomeric at pH 8.0 (Allen *et al.*, 1995).

All of the PRTs whose structures have been determined are oligomers in solution. Remarkably, however, great variation is seen in the oligomerization geometry: OPRT is the only PRT with a dimeric interface that resembles that of APRT. Structural alignment reveals that most of the APRT and OPRT dimer cores superimpose (r.m.s.d. on 188 C_α atoms is 2.9 Å, Figure 5B). The best alignment is at the central region of the APRT dimer, which corresponds to the entire OPRT dimer interface. This common interface is comprised of contacts between symmetry-related copies of H5 and contacts of the loop following H6 with H3 and the N-terminal two residues of H4 and H6. The superimposable dimer interfaces suggest that OPRT and APRT may represent a branch in the evolution of the type I PRT enzyme family that is distinct from the UPRTs and H/G/X/PRTs. This is consistent with the location of hood domains in the N-terminal region of APRT and OPRT, in contrast to the C-terminally located hood domains of other type I PRTs. The close structural similarity between APRT and OPRT is surprising, since type I PRT primary sequences are quite divergent and greater sequence similarity is not evident between APRT and OPRT.

Unlike OPRT, the *L.donovani* APRT dimer interface includes contacts from the C-terminal arm, which wraps around the neighboring monomer to contact β-strand S6, helix H9, the loop following H9, and H12 of the neighboring C-terminal arm. The C-terminal arm is responsible for burying almost half (1240 Å^2) of the total buried (2670 Å^2) solvent-accessible surface area upon dimer formation. It is possible that the arm contributes to catalysis by influencing the conformation of the flexible loop, since residues 220–226 of the arm contact the S6 β-strand, which immediately follows the flexible loop in the neighboring APRT monomer. The C-terminal arm appears to be unique to APRTs from *Leishmania*, and may provide an advantage to the parasite by increasing catalytic efficiency compared with the host enzyme. Curiously, protruding dimerization 'arms' are a feature of at least two other PRTs, XPRT (Vos *et al.*, 1997) and UPRT (Schumacher *et al.*, 1998), although these dimerization arms share neither topological nor structural similarity, nor are they peculiar to the parasite forms of the enzymes.

Ligand binding and recognition

Magnesium ion. Catalysis by APRT and the other type I PRTs requires magnesium. Type I PRT crystal structures show a Mg^{2+} coordinated to a conserved acidic dipeptide within the PRPP-binding motif (or via water molecules to the acidic dipeptide), as well as to the ribose hydroxyls and the β-phosphate of PRPP when PRPP is bound. A single magnesium ion was located in Ade–APRT and AMP–APRT at a position close to that of a magnesium ion in other PRT crystal structures (Ozturk *et al.*, 1995; Scapin *et al.*, 1995; Schumacher *et al.*, 1996; Krahn *et al.*, 1997; Vos *et al.*, 1997; Focia *et al.*, 1998b). This APRT Mg^{2+} site shows pseudo-octahedral coordination with ligands provided by the conserved side chain of Asp146 of the acidic dipeptide in the PRPP-binding motif and Thr154 $O_{\gamma 1}$ (although the Thr154 ligand is 3.7 Å distant in the AMP–APRT structure). Other ligands are provided by the ribose O3′ of AMP (or a water molecule in Ade–APRT), a citrate hydroxyl that may mimic a contact of the substrate β-phosphate group (3.31 Å in Ade–APRT;

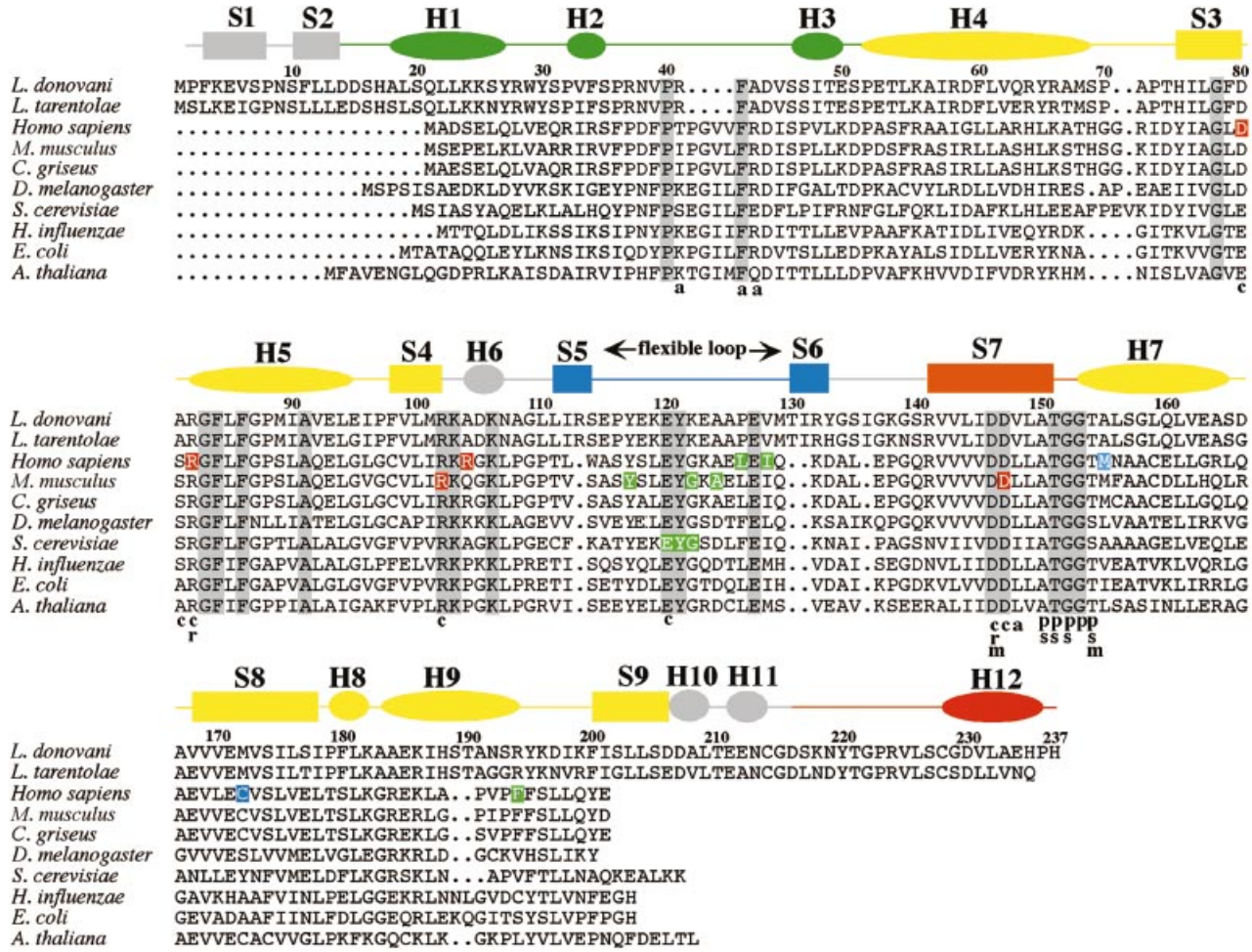

Fig. 4. Alignment of APRT sequences. Sequences were aligned using the program MultiAlign (Corpet, 1988). Residue numbering refers to the *L.donovani* sequence. Secondary structure of *L.donovani* APRT is indicated above, and colored as in Figure 3, with β-strands marked by rectangles and helices marked by ovals. Strand S1 (residues 3–7), S2 (10–13), S3 (75–79), S4 (98–101), S5 (111–113), S6 (130–132), S7 (141–150), S8 (168–177), S9 (200–205); Helix H1 (residues 18–26), H2 (32–34), H3 (46–49), H4 (52–68), H5 (82–94), H6 (104–106), H7 (153–164), H8 (179–181), H9 (183–190), H10 (205–208), H11 (211–213), H12 (228–235). The secondary structure assignments were used as defined by the program PROMOTIF (Hutchinson and Thornton, 1996) with the exceptions that helix H12 was lengthened at the C-terminus from residue 232 to 235, since this segment approximates a helical conformation, and helix H9 was shortened at the C-terminus from residue 193 to 190, since this region has an odd turn that does not appear to continue the helix smoothly. The N-terminal half of helix H5 (residues 82–88) is a 3_{10} helix, as are the short helices H2, H8, H10 and H11. The remaining helices are α-helices. Conserved residues are shaded gray. Residues that contact ligands are labeled under the sequences as follows: adenine 'a'; ribose 'r'; 5′-phosphate 'p'; magnesium 'm'; citrate 'c'; and sulfate (at the β-phosphate position) 's'. The human, mouse and *S.cerevisiae* APRT mutation positions discussed in the text are indicated with colored squares: red for mutations in regions that bind the β-phosphate of PRPP, green for mutations that apparently affect the conformation of the flexible loop, blue for mutations in the regions that bind the 5′ phosphate of PRPP. DDBJ/EMBL/GenBank database entries shown are *L.donovani* (409142); *Leishmania tarentolae* (3201678); *H.sapiens* (114074); *Mus musculus* (114075); *Cricetulus griseus* (486931); *Drosophila melanogaster* (479595); *S.cerevisiae* (1703347); *Haemophilus influenzae* (1574160); *E.coli* (1104073); *Arabidopsis thaliana* (2499931).

2.82 Å in AMP–APRT), and a water molecule that also hydrogen bonds to the main chain carbonyl oxygen of Asp80. The backbone of Asp80 is available for this interaction as a consequence of the unusual non-proline *cis*-peptide bond between Asp80 and Ala81, a feature conserved at the equivalent position in other PRT structures (*Escherichia coli* OPRT, *E.coli* XPRT, *Toxoplasma gondii* UPRT, *T.cruzi* HGPRT, *Tritrichomonas foetus* HGXPRT and *E.coli* GAT). An equivalent indirect metal ligand contact by the conserved *cis*-peptide backbone carbonyl via a water molecule is also seen in the GAT–PRPP complex (Krahn *et al.*, 1997). A potential sixth magnesium ligand is the carboxylate of Glu127 in the flexible loop, which is 5 Å from the magnesium in the AMP–APRT structure but may coordinate the magnesium when the loop adopts a closed conformation.

A second magnesium ion is seen in a ternary complex of *T.cruzi* HGPRT with PRPP and a hypoxanthine analog (Focia *et al.*, 1998b). This ion coordinates an aspartate side chain of the hood as well as the hypoxanthine analog N_3 via an ordered water molecule, potentially positioning the purine base for nucleophilic attack at the PRPP ribose C1′. We see no evidence of a magnesium ion bound at this position in the APRT structures, nor are there any obvious acidic ligands available for coordination in this rather hydrophobic pocket of APRT.

Sulfate and citrate anions. One of the two sulfate ions

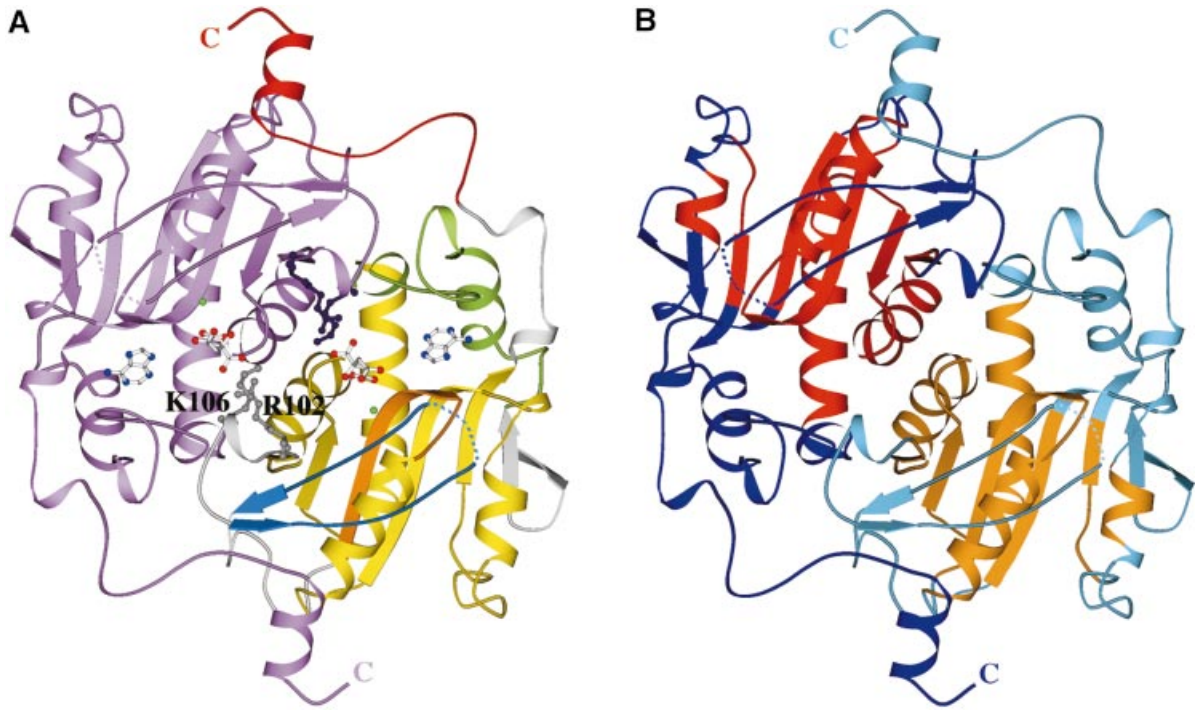

Fig. 5. Ribbon diagrams of the Ade–APRT dimer. (**A**) One subunit is colored as in Figure 3, and the other subunit is purple. The adenine and citrate are gray with the oxygen atoms red and the nitrogen atoms blue. Adenine is shown in the 'A' orientation. The magnesium ion is green. Arg102 and Lys106 side chains are shown in ball-and-stick representation, with those belonging to the purple monomer colored dark purple, and those belonging to the multi-colored monomer in gray. (**B**) APRT molecules shown in dark blue and light blue, with the region that superimposes with the OPRT dimer in red and orange. The superposition was performed for the APRT dimer onto the OPRT dimer from *S.typhimurium* (PDB accession code 1OPR) (Scapin *et al.*, 1995), with equivalent residues from both monomers of the dimers included in the least squares fit. The equivalent residues, given for one monomer only, are 54–94, 95–102, 140–165, 168–174, 183–188 and 197–202 of APRT with 45–85, 92–99, 118–143, 146–152, 166–172 and 175–180 of OPRT. The least squares fitting routine in the program O (Jones, 1991) was used for the superposition, and gave an r.m.s.d. of 2.9 Å on C_α atoms.

found in the apo-AS–APRT structure is in the same place as the phosphate moiety of AMP in the AMP–APRT structure (below). The other sulfate overlaps with the site occupied by a citrate ion in the apo–, Ade– and AMP–APRT structures. We speculate that this second sulfate corresponds to the binding site for the β-phosphate group of the substrate PRPP. Both of these equivalent sites are also occupied by sulfate anions in the crystal structures of *E.coli* OPRT (Henriksen *et al.*, 1996), *E.coli* XPRT (Vos *et al.*, 1997) and *T.gondii* UPRT (Schumacher *et al.*, 1998). Binding of sulfates at the phosphate-binding sites explains our failure to prepare co-crystal complexes of apo-AS–APRT with substrates or products.

The citrate anion seen in apo–, Ade– and AMP–APRT (Figures 2C, 7 and 8) probably mimics binding of the product pyrophosphate and the pyrophosphate moiety of the PRPP substrate. Like pyrophosphate, citrate has hydrogen bond-accepting oxygen atoms and tetrahedral coordination, although unlike pyrophosphate, citrate does not carry a highly negative charge, has protonated oxygen atoms, and is somewhat larger. The electron density for citrate was very clear in the Ade– and apo–APRT structures but rather poorly defined in AMP–APRT, where relatively high B-values (55 $Å^2$) possibly reflect partial occupancy caused by limited space for the large citrate molecule in the presence of AMP.

Contacts to the citrate include hydrogen bonds from the guanidinium $N_{\eta 2}$ of Arg82 and the backbone amides

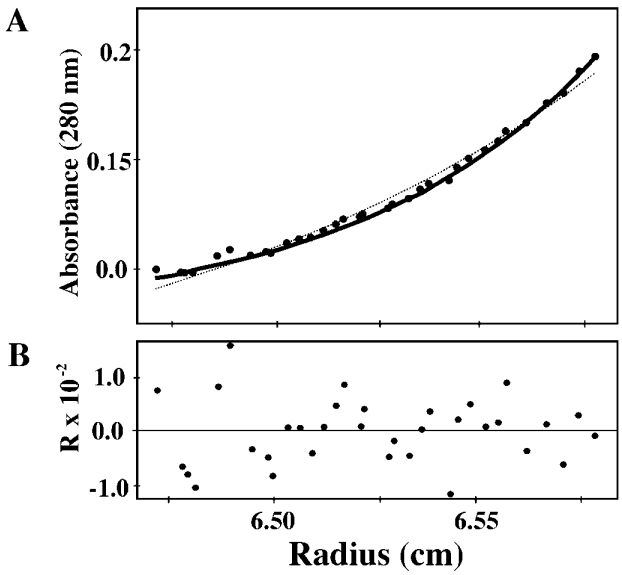

Fig. 6. Equilibrium sedimentation analysis of APRT. (**A**) The dark line is a fit of the data to a dimer of 52 kDa. The dotted line is the poor observed fit assuming a monomer of 26 kDa. (**B**) Residuals for the data in (A) when fit to a dimer. This scan was collected at 23 000 r.p.m., 280 nm on protein at 0.4 mg/ml, pH 6.5.

of Arg82 and *cis*-Ala81 (Figures 7 and 8). Notably, Arg102 and Lys106 from the neighboring molecule in the dimer also make contact with citrate and sulfate bound at the PRPP β-phosphate position; Arg102 $N_{\eta 2}$ donates two hydrogen bonds to sulfate and citrate, while Lys106 N_{ζ} hydrogen bonds the sulfate and is within 4 Å of the citrate. Although these residues are not conserved in hypoxanthine, guanine, xanthine or uracil PRTs, they are *invariant* across APRTs (Figure 4) and OPRTs, which are the only PRTs known to share the APRT dimer structure (above). The equivalent Arg and Lys residues of *Salmonella typhimurium* OPRT make the same contacts to the β-phosphate of bound PRPP (Scapin *et al.*, 1995). Furthermore, biochemical complementation studies on *S.typhimurium* OPRT showed that this lysine is required for catalysis in the symmetry-related active site (Ozturk *et al.*, 1995), and a glutamine substitution at the equivalent arginine position in mouse APRT (Figures 4 and 9) results in lowered specific activity and slightly higher K_m for PRPP (Khattar *et al.*, 1995). These observations strongly suggest that dimerization is required for catalysis by APRT.

It is likely that Arg102 and Lys106 function to neutralize negative charge on the β-phosphate moiety in the transition state for 5′-phosphoribosyl transfer. These residues are well suited to accommodate the conformational changes expected during the enzymatic reaction. Indeed, in *S.typhimurium* OPRT, the anomeric carbon of the ribose moiety moves 7 Å across the binding cavity in the PRPP–orotate complex relative to the OMP complex (Scapin *et al.*, 1994, 1995). It is notable that although all type I PRTs have a common core domain and bind PRPP for 5-phosphoribosyl transfer, only APRT and OPRT have this β-phosphoryl-binding loop from a symmetry-related subunit.

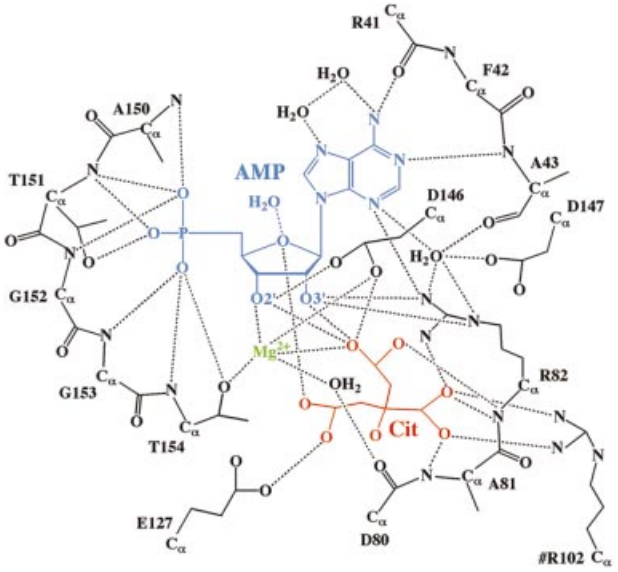

Fig. 7. Schematic representation of contacts to AMP. Hydrogen bonds and metal–ligand contacts are indicated with a dotted line and defined as for Figure 8.

AMP. The AMP–APRT structure reveals the AMP product bound in the low energy *anti* conformation with the ribose in the *2′ endo* conformation (Figures 7 and 8). The hood region provides nearly all of the contacts to the adenine base, including the hydrogen bonds (Ade $N_{\eta 2}\cdots$Arg41 O, and Ade $N_1\cdots$Ala43 N), which define specificity for adenine over other purines lacking these hydrogen bonding groups. The AMP is sandwiched between the hydrophobic groups of Phe42 and Val148. Unlike other purine- and pyrimidine-binding PRTs, Val148 is the only core residue of APRT that makes direct contact with the base.

Type I PRTs that bind hypoxanthine, guanine, xanthine, or orotate select substrate, in part, on the basis of a hydrogen bond between the purine 6-oxo or pyrimidine 4-oxo group and a basic side chain just C-terminal to the fourth β-strand of the PRT core (S8 in APRT). Indeed, a mutation of this residue, Lys134Ser, enables *T.foetus* HGXPRT to bind adenine (Munagala and Wang, 1998). However, consistent with the specificity for adenine, the corresponding residue in *L.donovani* APRT is Ile178, which cannot hydrogen bond and lies 6.0 Å distant from

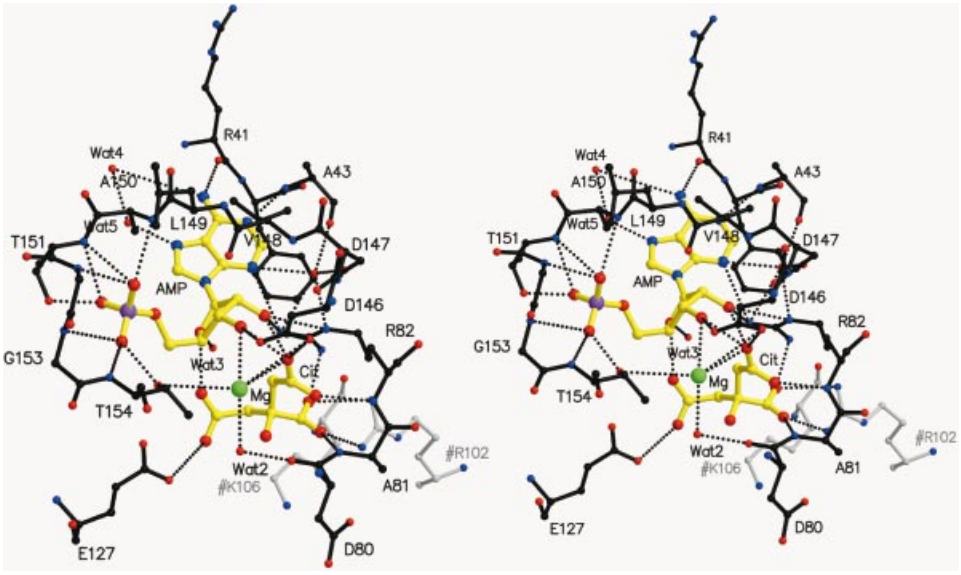

Fig. 8. Stereo diagram of the active site of AMP–APRT. The AMP and citrate are yellow. The magnesium is green. The surrounding protein from the APRT monomer is black. The cross-dimer contacting residues, #R102 and #K106, are gray. Hydrogen bond and metal ligand contacts are indicated with a dotted line (hydrogen bonds <3.2 Å, metal ligands <2.9 Å, except $Mg^{2+}\cdots$154Thr $O_{\gamma 1}$ at 3.7 Å, see text).

the adenine base in the Ade– and AMP–APRT structures. Moreover, all of the C-terminal end of APRT S8 is distant from the adenine and there are no adenine contacts from this region. Thus, in contrast to hypoxanthine, xanthine, guanine and orotate PRTs, this region of the APRT core does not contribute to base binding or specificity.

As seen in other PRT structures, the AMP phosphate and ribose groups are bound by the highly conserved PRPP-binding motif. Hydrogen bonds are made to the AMP phosphate by the backbone amides of Ala150, Thr151, Gly152, Gly153 and Thr154, and the OH groups of Thr151 and Thr154. Hydrogen bonds to the AMP ribose 2′OH and 3′OH are made by the side chains of Asp146 and Asp147, respectively. A conservative glutamate substitution for Asp147 at the equivalent position in mouse APRT (Figures 4 and 9) results in a dramatic loss in affinity for PRPP, and mutation to tyrosine results in a complete loss of APRT activity (Khattar *et al.*, 1995). This acidic residue appears to play a crucial role in PRPP binding of the ribose hydroxyls, either directly, or through the magnesium ion (see magnesium ion section above).

In HGPRTs, a Ser–Tyr dipeptide in the flexible loop is believed to be necessary for protection of the proposed oxocarbonium ion transition state, and may directly contact the PRPP ribose during the reaction (Schumacher *et al.*, 1996; Eads *et al.*, 1997). Biochemical studies of mutations and chemical modifications at this dipeptide in *L.donovani* HGPRT result in dramatic lowering of the k_{cat} (Jardim and Ullman, 1997). The *L.donovani* APRT Glu120 and Tyr121 (Figures 4 and 9) in the flexible loop may play a similar role, and these residues are conserved across APRTs (Figure 4). Indeed mutation of the equivalent residues in *Saccharomyces cerevisiae* APRT (Glu106Leu and Tyr107Asp) also results in dramatically lowering the k_{cat} for the reaction (Crother and Taylor, 1998).

Adenine. There are two regions of local change between the Ade–APRT and AMP–APRT structures (Figure 10). The 5′-phosphate-binding loop, residues 147–154, moves by ~1.0 Å to accommodate the 5′-phosphate of AMP, and the Arg82 guanidinium shifts by 1.4 Å to accommodate the AMP ribose.

Remarkably, the 1.5 Å resolution electron density for Ade–APRT indicated that the adenine was bound in two alternative conformations, which we have modeled as each having 50% occupancy (Figures 2A, 2B and 8). In both orientations, adenine stacks against Phe42 and Val148, as seen for AMP–APRT. In orientation ‘A’, the adenine appears to be suitably positioned for the catalytic reaction, i.e. the reactive N_9 is proximal to the expected position of the PRPP ribose. Curiously, the hydrogen bonds seen in this orientation (Ade N_1···Arg41 O and Ade N_3···Ala43 O) do not explain the specificity of APRT for adenine over other purines, such as hypoxanthine, xanthine or guanine, all of which could apparently provide the equivalent hydrogen bonds with no unfavorable contacts. In contrast, orientation ‘B’ is not suitable for reaction with PRPP but does include hydrogen bonding contacts (Ade N_1···Ala43 N_η and Ade $N_{\eta 2}$···Ala43 O) that are specific for adenine. As seen in the AMP–APRT complex, Arg82 $N_{\eta 2}$ contacts the N_3 of the adenine, but only in orientation ‘B’.

Our initial expectation was that adenine alone would bind in the same manner as the adenine moiety of AMP, which seems to adopt a catalytically relevant conformation that includes base-specific hydrogen bonds. However, the electron density clearly indicates that this is not the case. Modeling of adenine into the orientation seen for AMP increases R_{free}, and positional refinement moves the adenine into orientation ‘A’. It is possible that the Ade–APRT structure is an artifact of crystallization, and that in solution the adenine may bind as observed for AMP, although the ability of AMP and adenine to bind in isomorphous crystals argues against this possibility. It is also possible that the catalytic ‘A’ orientation is only accessible to adenine following specific binding in the ‘B’ orientation, although the basis for this is not apparent from the crystal structures. Alternatively, it is possible that the specificity of APRT for adenine does not result from favorable hydrogen bonding interactions but owes more to steric limitations on positioning or reacting alternative bases in the active site. Finally, it is possible that adenine specificity derives from additional interactions formed only when the flexible loop is in the closed conformation. This idea is supported by biochemical data showing reduced adenine affinity in mouse (Khattar *et al.*, 1995) and *S.cerevisiae* (Crother and Taylor, 1998) APRTs with mutations of residues equivalent to *L.donovani* APRT 117, 122 and 124 (Figures 4 and 9), all of which are located at the tip of the flexible loop and could reach the adenine binding site if the loop adopts a closed conformation.

There are no obvious candidates for abstracting the adenine N_9 proton when the flexible loop is in the open conformation. However, two glutamate residues in the flexible loop, Glu120 and Glu127, are completely conserved across APRTs and could reach the adenine-binding site when the loop is closed. These residues are therefore good candidates for performing proton abstraction upon loop closure.

Correlation of clinical mutations with structure

At least seven missense mutations and one codon deletion in human APRT are associated with renal dysfunction due to 2,8-dihydroxyadenine stone formation, a rare form of kidney stones (Simmonds *et al.*, 1995). The *L.donovani* APRT crystal structure explains why human APRT activity may be impaired with most of these mutations, although in most cases it is possible that the effect is more indirect, for example due to increased turnover of RNA or protein. The mutations cluster in three regions of APRT: the regions that bind the β-phosphate of PRPP, the 5′ phosphate of PRPP, and the region of the flexible loop proposed to close over the active site during catalysis (Figures 4 and 9).

The Asp65Val mutation is in the region that apparently binds the PRPP β-phosphate. The carboxylate of the equivalent *L.donovani* Asp80 side chain hydrogen bonds the backbone N_η of *cis*-Ala81, thereby stabilizing the conserved *cis*-peptide conformation that functions in coordination of the magnesium ion and the β-phosphate of PRPP. The Asp80 carboxylate also hydrogen bonds the N_ε and $N_{\eta 2}$ of Arg102, a residue that makes contacts across the dimer interface to the cross-subunit β-phosphate of PRPP (citrate, sulfate in these APRT structures). Substitution of aspartate by valine at this position would result in the absence of these active site hydrogen bonds, and

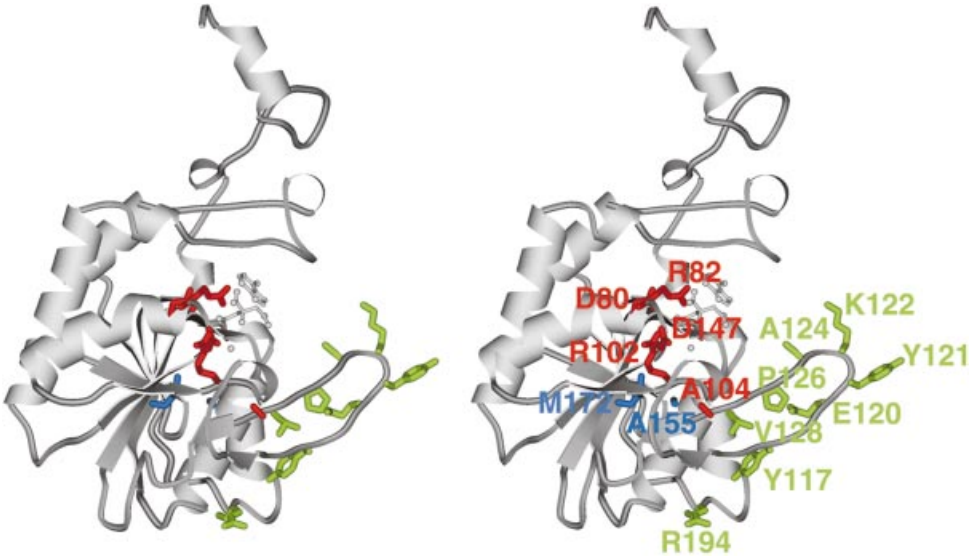

Fig. 9. Stereo ribbon diagram of monomer Ade–APRT showing mutated residues. Green, mutated positions that apparently affect the conformation of the flexible loop region; red, residues mutated in the β-phosphate binding region; blue, residues mutated in the 5′ phosphate binding region. Colors correspond to those in Figure 4. The orientation is similar to that for Figure 3A.

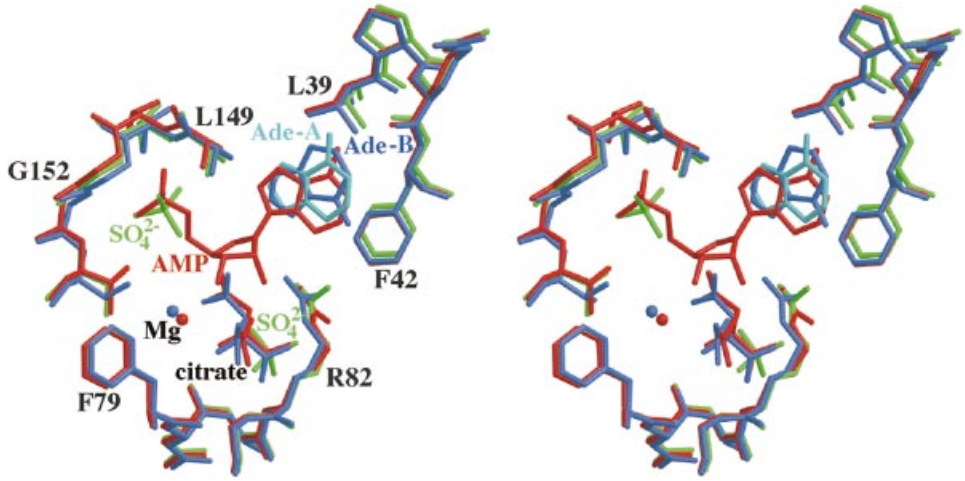

Fig. 10. Superposition of APRT active site structures. AMP–APRT red; apo-AS–APRT green; Ade–APRT A orientation light blue; Ade–APRT B orientation dark blue.

would probably alter PRPP binding and/or reactivity. Substitution of the adjacent residue Arg67Gln, which is equivalent to Arg82 of *L.donovani*, also results in APRT deficiency disease. This guanidinium hydrogen bonds to the ribose hydroxyls in the AMP–APRT structure, and substitution of this residue probably disrupts contacts to the PRPP substrate. The Arg89Gln mutation in human APRT, which is associated with renal disease and is equivalent to Ala104 in *L.donovani* APRT, may also disrupt the cross-subunit contacts to the PRPP β-phosphate made by nearby *L.donovani* Arg102 and Lys106 (Figures 4 and 9).

The *L.donovani* APRT structures also suggest why human APRT function is compromised in people with a Met136Thr mutation, the most common APRT human missense mutation (Simmonds *et al.*, 1995). The equivalent *L.donovani* APRT residue, Ala155, is buried adjacent to Leu149 (Figures 7 and 8). Human APRT Met136 presumably packs in a similarly close-packed environment, and substitution with the β-branched threonine side chain is expected to disrupt the conformation of the intervening 5′-phosphate binding loop of residues 150–154 in the PRPP-binding motif. Indeed, human Met136Thr APRT binds PRPP with lower affinity in a biochemical assay (Fujimori *et al.*, 1985, 1986). Likewise, the human Cys153Arg mutation (equivalent to Met172 in *L.donovani* APRT) probably changes the conformation of the 5′ phosphate binding loop, since the side chain of Met172 is also buried against Ala155.

The third region of human APRT with clinically relevant mutations is the flexible loop, where the mutations Leu110Pro and Ile112Phe are associated with renal dysfunction in humans. These residues align with *L.donovani* APRT Pro126 and Val128. Three nearby residues (117, 122 and 124) have been implicated in adenine binding in biochemical studies on mouse (Khattar *et al.*, 1995) and *S.cerevisiae* (Crother and Taylor, 1998) APRTs. The clinical effects of these mutations are not obvious from

the *L.donovani* APRT structures, although they may disrupt the active closed conformation of the flexible loop. Deletion of human Phe173, corresponding to Arg194 in *L.donovani* APRT, is also associated with renal dysfunction. This residue lies at the C-terminus of helix H9, a region that is very close to the open flexible loop, and possibly stabilizes this conformation for substrate binding. Indeed, *L.donovani* APRT Tyr117 O_η is only 3.5 Å from Thr190 $C_{\gamma2}$ and $O_{\gamma1}$.

Structural differences between *L.donovani* APRT and human APRT may provide a basis for the development of anti-parasite therapies. The considerably smaller human APRT lacks the two N-terminal β-strands S1 and S2, as well as the C-terminal S9 strand, H10, H11 and H12 helices (Figure 4). Therefore, the twisted β-sheet core of the human enzyme is three β-strands shorter and there is no contribution to the dimerization interface by a C-terminal arm. There also appears to be a significant difference at the active site, where non-*Leishmania* APRTs apparently possess a four residue insertion between Arg41 and Phe42 of *L.donovani* APRT. This may provide variation on the adenine binding scaffold and thereby provide an attractive basis for the development of specific therapeutic agents.

Materials and methods

Protein preparation and crystallization

Leishmania donovani APRT was purified as described (Phillips *et al.*, 1996), and concentrated (Gill and von Hippel, 1989) to 10 mg/ml in 10 mM MES pH 6.0, 1 mM dithiothreitol and 5 mM $MgCl_2$. Crystals were grown at 4°C by vapor diffusion in 12–16 μl hanging drops comprised of equal volumes of APRT and reservoir solutions. The reservoir solution for apo-AS–APRT crystals was 1.2–1.6 M $(NH_4)_2SO_4$, 0.1 M sodium citrate pH 4.9 and 10 mM $MgCl_2$. Prior to data collection, these crystals were equilibrated at room temperature for 1–2 h and mounted in capillaries. Apo–APRT crystals were grown at 4°C using a reservoir of 7–11% PEG 5000 monomethyl ether (MME), 0.2 M ammonium acetate, 0.1 M sodium citrate, pH 5.0, 10 mM $MgCl_2$. AMP- and adenine-bound APRT crystals were grown from the same conditions with either 10 mM AMP or 5 mM adenine in the reservoir solution. Crystals grown in either $(NH_4)_2SO_4$ or in PEG 5000 MME grew to full size (typically 0.4×0.4×0.7 mm) within 2–4 weeks.

Data collection and processing

APRT crystals belong to space group $P6_122$, with one molecule in the asymmetric unit and a solvent content of 55% (Matthews, 1968). Data for native and derivative apo-AS–APRT crystals were collected at room temperature on an Area Detector Systems Corporation (ADSC) multiwire detector (Xuong *et al.*, 1985) with a RIGAKU RU200-H rotating anode X-ray source and processed with the software provided by ADSC. Details are described elsewhere (Phillips *et al.*, 1996).

Data collection was performed at 100 K for the apo–, AMP– and Ade–APRT crystals grown with PEG as the precipitant. Crystals were cryoprotected by brief immersion in reservoir solution made to 20% glycerol, suspended in a rayon loop and cooled by plunging into liquid nitrogen. Cryocooling shrunk the crystals by ~5 Å along the *c* axis, but room temperature and frozen crystals were otherwise isomorphous. Data from the AMP- and adenine-bound APRT crystals were collected at a wavelength of 1.08 Å on a MAR Research detector at beam line 7-1 of the Stanford Synchrotron Radiation Laboratory. Data from the apo–APRT crystal were collected on a Rigaku R-AXIS IV imaging plate area detector with a mirror-focused Rigaku RU-200 copper target rotating anode X-ray source operating at 5 kW. Data from cryocooled crystals were processed with the programs DENZO and SCALEPACK (Otwinowski and Minor, 1997).

Structure determination and refinement

Crystallographic calculations employed programs from the CCP4 suite (Dodson *et al.*, 1997) except where noted. The structure of apo-AS–APRT was determined by multiple isomorphous replacement methods using $HgCl_2$ and selenomethionine derivatives. Heavy atom sites were located by difference Patterson and Fourier synthesis, and refined using the program PHASES (Furey and Swaminathan, 1995) to give a mean figure of merit of 0.59 for data to 3.0 Å resolution (Table III). Solvent flattening using PHASES gave a mean figure of merit of 0.85 and an electron density map into which a partial polyalanine model was built with O (Jones *et al.*, 1991). The map was improved by several rounds of map fitting and phase combination. Rounds of rebuilding and refinement with X-PLOR (Brünger, 1996) gave the final apo-AS–APRT model, which has an *R*-value of 17.6% (R_{free} 25.0%) for all data to 2.48 Å resolution (Table IV).

The refined apo-AS–APRT model, excluding solvent, was used as a starting model for refinement of the Ade–APRT structure. The refined structure includes an adenine, a magnesium ion and a citrate ion. The adenine could be modeled into electron density maps in two mutually exclusive overlapping orientations. No change in R_{free} was observed following refinement using either or both adenine orientations, and both orientations are included in the final model with occupancies of 0.5. The refined structure has an *R*-value of 20.0% (R_{free} 23.9%).

The adenine–APRT structure, without ligands or water molecules, was used as the starting model for refinement of the AMP–APRT and apo–APRT structures. The AMP was well defined in the $[(F_o–F_c), \phi_{calc}]$ electron density map. The sugar pucker was unrestrained during refinement, and remained clearly in the C2′-*endo* conformation. Like Ade–APRT, both AMP–APRT and apo–APRT contain a bound citrate ion, although this is less well defined in AMP–APRT. The AMP–APRT structure has a final *R*-value of 19.6%, and an R_{free} of 26.3%. The apo–APRT structure has a final *R*-value of 18.7%, and an R_{free} of 24.1%. Coordinates and structure factors for all the APRT structures have been deposited with the Brookhaven Protein Data Bank (PDB accession codes: Ade–APRT, 1QB7; AMP–APRT, 1QB8; apo–APRT, 1QCC; apo-AS–APRT, 1QCD).

Equilibrium centrifugation

Equilibrium centrifugation experiments were performed using a Beckman XL-A Optima analytical centrifuge. Samples at lower protein concentrations of 0.065, 0.0325 and 0.0163 mg/ml were analyzed in 10 mM potassium phosphate pH 6.5 and scanned at 230 nm. Samples at higher protein concentrations of 0.2, 0.3 and 0.4 mg/ml were analyzed in 20 mM MES pH 6.5, 5 mM $MgCl_2$ and scanned at 280 nm. Samples were spun at 15 000, 18 000, 20 000, 23 000, 25 000 and 42 000 r.p.m. Scans were taken at each speed until equilibrium was reached, as judged by superimposable consecutive scans. The protein was fully sedimented at 42 000 r.p.m.. Background absorbance was corrected empirically by allowing the baseline to float during the fitting calculations, and an estimated partial specific volume of 0.73 ml/g was used to fit the data using software provided with the instrument.

Acknowledgements

We thank Anna Paulsen for help with analytical centrifugation, light scattering experiments, and protein purification; Armando Jardim for N-terminal sequencing; Felix Vajdos and David Worthylake for advice regarding crystallography; Henry Bellamy, Randolph Knowlton, Peter Kuhn, and Michael Mathews for assistance with synchrotron data collection. This work was supported by N.I.H. grants GM50163 (C.P.H.) and AI23682 (B.U.). C.L.P. was a Burroughs Wellcome Fund Life Sciences Research Fellow. B.U. is a Burroughs Wellcome Fund Scholar in Molecular Parasitology, and this work was supported in part by a grant from the Burroughs Wellcome Fund.

References

Allen,T., Hwang,H.-Y., Wilson,K., Hanson,S., Jardim,A. and Ullman,B. (1995) Cloning and expression of the adenine phosphoribosyltransferase gene from *Leishmania donovani*. *Mol. Biochem. Parasitol.*, **74**, 99–103.

Argos,P., Hanei,M., Wilson,J.M. and Kelley,W.N. (1983) A possible nucleotide-binding domain in the tertiary fold of phosphoribosyltransferases. *J. Biol. Chem.*, **258**, 6450–6457.

Berens,R.L., Krug,E.C. and Marr,J.J. (1995) *Purine and Pyrimidine Metabolism*. Academic Press, London, UK.

Bhatia,M.B., Vinitsky,A. and Grubmeyer,C. (1990) Kinetic mechanism of orotate phosphoribosyltransferase from *Salmonella typhimurium*. *Biochemistry*, **29**, 10480–10487.

Brünger,A.T. (1996) X-PLOR version 3.843, a system for X-ray crystallography and NMR. Yale University, New Haven, CT.

Corpet,F. (1988) Multiple sequence alignment with hierarchical clustering. *Nucleic Acids Res.*, **16**, 10881–10890.

Crother,T.R. and Taylor,M.W. (1998) Site directed mutagenesis of the *Saccharomyces cerevisiae* APT1 gene. In Griesmacher,A., Chiba,P. and Müller,M.M. (eds) *Purine and Pyrimidine Metabolism in Man IX*. Plenum Press, New York, NY, Vol. 431, pp. 299–303.

de Boer,J.G. and Glickman,B.W. (1991) Mutational analysis of the structure and function of the adenine phosphoribosyltransferase enzyme of Chinese hamster. *J. Mol. Biol.*, **221**, 163–174.

Dodson,E.J., Winn,M. and Ralph,A. (1997) Collaborative computational project, number 4: Providing programs for protein crystallography. *Methods Enzymol.*, **277**, 620–633.

Eads,J.C., Scapin,G., Xu,Y., Grubmeyer,C. and Sacchettini,J.C. (1994) The crystal structure of human hypoxanthine-guanine phosphoribosyltransferase with bound GMP. *Cell*, **78**, 325–334.

Eads,J.C., Ozturk,D., Wexler,T.B., Grubmeyer,C. and Saccettini,J.C. (1997) A new function for a common fold: the crystal structure of quinolinic acid phosphoribosyltransferase. *Nature Struct. Biol.*, **5**, 47–58.

Focia,P.J., Sydney,P.C.,III, Nieves-Alicea,R., Fletterick,R.J. and Eakin,A.E. (1998a) A 1.4 Å crystal structure for the hypoxanthine phosphoribosyltransferase of *Trypanosoma cruzi*. *Biochemistry*, **37**, 15066–15075.

Focia,P.J., Craig,S.P.,III and Eakin,A.E. (1998b) Approaching the transition state in the crystal structure of a phosphoribosyltransferase. *Biochemistry*, **37**, 17120–17127.

Fujimori,S., Akaoka,I., Sakamoto,K., Yamanaka,H., Nishioka,K. and Kamatani,N. (1985) Common characteristics of mutant adenine phosphoribosyltransferase from four separate Japanese families with, 2,8-dihydroxyadenine urolithiasis associated with partial enzyme deficiencies. *Hum. Genet.*, **71**, 171–176.

Fujimori,S., Akaoka,I., Takeuchi,F., Kanayama,H., Tatara,K., Nishioka,K. and Kamatani,N. (1986) Altered kinetic properties of a mutant adenine phosphoribosyltransferase. *Metabolism*, **35**, 187.

Furey,W. and Swaminathan,S. (1997) PHASES-95: A program package for processing and analyzing diffraction data from macromolecules. *Methods Enzymol.*, **277**, 590–620.

Gill,S.C. and von Hippel,P.H. (1989) Calculation of extinction coefficients from amino acid sequence data. *Anal. Biochem.*, **182**, 319–326.

Henriksen,A., Aghajari,N., Jensen,K.F. and Galhede,M. (1996) A flexible loop at the dimer interface is a part of the active site of the adjacent monomer of *Escherichia coli* orotate phosphoribosyltransferase. *Biochemistry*, **35**, 3803–3809.

Hershey,H.V. and Taylor,M.W. (1986) Nucleotide sequence and deduced amino acid sequence of *Escherichia coli* adenine phosphoribosyltransferase and comparison with other analogous enzymes. *Gene*, **43**, 287–293.

Hove-Jensen,B., Harlow,K.W., King,C.J. and Switzer,R.L. (1986) Phosphoribosyl-pyrophosphate synthetase of *Escherichia coli*: properties of the purified enzyme and primary structure of the prs gene. *J. Biol. Chem.*, **261**, 6765–6771.

Hubbard,S.J. and Thornton,J.M. (1993) NACCESS. Department of Biochemistry and Molecular Biology, University College London.

Hutchinson,E.G. and Thornton,J.M. (1996) PROMOTIF—a program to identify and analyze structural motifs in proteins. *Protein Sci.*, **5**, 212–220.

Hwang,H. and Ullman,B. (1997) Genetic analysis of purine metabolism in *Leishmania donovani*. *J. Biol. Chem.*, **272**, 19488–19496.

Jardim,A. and Ullman,B. (1997) The conserved serine-tyrosine dipeptide in *Leishmania donovani* hypoxanthine-guanine phosphoribosyltransferase is essential for catalytic activity. *J. Biol. Chem.*, **272**, 8967–8973.

Jones,T.A., Zou,J.Y., Cowan,S.W. and Kjeldgaard,M. (1991) Improved methods for building protein models in electron density maps and the location of errors in these models. *Acta Crystallogr.*, **A47**, 110–119.

Khattar,N.H., Jennings,C.D., Walker,K.A. and Turker,S.T. (1995) Isolation and characterization of mutations in the mouse APRT gene that encode functional enzymes with resistance to toxic adenine analogs. In Sahota,A. and Taylor,M.W. (eds) *Purine and Pyrimidine Metabolism in Man VIII*. Plenum Press, New York, NY, Vol. 370, pp. 665–670.

Krahn,J.M., Kim,J.H., Burns,M.R., Parry,R.J., Zalkin,H. and Smith,J. (1997) Coupled formation of an amidotransferase interdomain ammonia channel and a phosphoribosyltransferase active site. *Biochemistry*, **36**, 11061–11068.

Kraulis,P.J. (1991) MOLSCRIPT: a program to produce both detailed and schematic plots of structures. *J. Appl. Crystallogr.*, **24**, 946–950.

Laskowski,R.A., MacArthur,M.W. and Thornton,J.M. (1993) PROCHECK: a program to check the stereochemical quality of protein structures. *J. Appl. Crystallogr.*, **26**, 283–291.

Looker,D.L., Berens,R.L. and Marr,J.J. (1983) Purine metabolism in *Leishmania donovani* amastigotes and promastigotes. *Mol. Biochem. Parasitol.*, **9**, 15–23.

Matthews,B.W. (1968) Solvent content of protein crystals. *J. Mol. Biol.*, **33**, 491–497.

Muchmore,C.R., Krahn,J.M., Kim,J.H., Zalkin,H. and Smith,J.L. (1998) Crystal structure of glutamine phosphoribosylphosphate amidotransferase from *Escherichia coli*. *Protein Sci.*, **7**, 39–51.

Munagala,N.R. and Wang,C.C. (1998) Altering the purine specificity of hypoxanthine-guanine-xanthine phosphoribosyltransferase from *Tritrichomonas foetus* by structure-based point mutations in the enzyme protein. *Biochemistry*, **37**, 16612–16619.

Musick,W.D.L. (1981) Structural features of the phosphoribosyltransferases and their relationship to the human deficiency disorders of purine and pyrimidine metabolism. *CRC Crit. Rev. Biochem.*, **11**, 1–34.

Otwinowski,Z. and Minor,W. (1997) Processing of X-ray diffraction data collected in oscillation mode. *Methods Enzymol.*, **276**, 307–326.

Daresbury Laboratory, Warrington, UK, pp. 56–62.

Ozturk,D.H., Dorfman,R.H., Scapin,G., Sacchettini,J.C. and Grubmeyer,C. (1995) Structure and function of *Salmonella typhimurium* orotate phosphoribosyltransferase: protein complementation reveals shared active sites. *Biochemistry*, **34**, 10764–10770.

Phillips,C.L., Ullman,B. and Brennan,R.G. (1996) Crystallization of the purine salvage enzyme adenine phosphoribosyltransferase. *Proteins Struct. Funct. Genet.*, **25**, 510–513.

Pillwein,K. *et al*. (1990) Purine metabolism of human glioblastoma *in vivo*. *Cancer Res.*, **50**, 1576–1579.

Scapin,G., Grubmeyer,C. and Sacchettini,J.C. (1994) Crystal structure of orotate phosphoribosyltransferase. *Biochemistry*, **33**, 1287–1294.

Scapin,G., Ozturk,D.H., Grubmeyer,C. and Sacchettini,J.C. (1995) The crystal structure of the orotate phosphoribosyltransferase complexed with orotate and α-D-5-phosphoribosyl-L-phosphate. *Biochemistry*, **34**, 10744–10754.

Schumacher,M.A., Carter,D., Roos,D., Ullman,B. and Brennan,R.G. (1996) Crystal structures of *Toxoplasma gondii* HGXPRTase reveal the catalytic role of a long flexible loop. *Nature Struct. Biol.*, **3**, 881–887.

Schumacher,M.A., Carter,D., Scott,D.M., Roos,D., Ullman,B. and Brennan,R.G. (1998) Crystal structure of *Toxoplasma gondii* uracil phosphoribosyltransferase reveal the atomic basis of pyrimidine discrimination and prodrug binding. *EMBO J.*, **17**, 3219–3232.

Simmonds,H.A., Sahota,A.S. and Van Acker,K.J. (1995) Adenine phosphoribosyltransferase deficiency and 2,8-dihydroxyadenine lithiasis. In Scriver,C.R., Beaudet,W.S., Sly,W.S. and Valle,D. (eds), *The Metabolic and Molecular Bases of Inherited Disease*. McGraw-Hill, New York, NY, pp. 1707–1724.

Smith,J.L., Zaluzee,E.J., Wery,J.P., Niu,L., Switzer,R.L., Zalkin,H. and Satow,Y. (1994) The structure of the allosteric regulatory enzyme of purine biosynthesis. *Science*, **264**, 1427–1433.

Somoza,J.R., Chin,M.S., Focia,P.J., Wang,C.C. and Fletterick,R.J. (1996) Crystal structure of the hypoxanthine-guanine-xanthine phosphoribosyltransferase from the protozoan parasite *Tritrichomonas foetus*. *Biochemistry*, **35**, 7032–7040.

Vos,S., de Jersey,J. and Martin,J.L. (1997) Crystal structure of *Escherichia coli* xanthine phosphoribosyltransferase. *Biochemistry*, **36**, 4125–4134.

Wang,G.P., Lundegaard,C., Jensen,K.F. and Grubmeyer,C. (1999a) Kinetic mechanism of OMP synthase: A slow physical step following group transfer limits catalytic rate. *Biochemistry*, **38**, 275–283.

Wang,G.P., Cahill,S.M., Liu,X., Girvin,M.E. and Grubmeyer,C. (1999b) Motional dynamics of the catalytic loop in OMP synthase. *Biochemistry*, **38**, 284–295.

Weber,G., Jayaram,H.M., Pillwein,K., Natsumeda,Y., Reardon,M.A. and Zhen,W.S. (1987) Salvage pathways as targets of chemotherapy. *Adv. Enzyme Regul.*, **26**, 335–352.

Xuong,N.H., Nielson,C., Hamlin,R. and Anderson,D.J. (1985) Strategy for data collection from protein crystals using a multiwire counter area detector diffractometer. *J. Appl. Crystallogr.*, **18**, 342–350.

Yuan,L., Craig,S.P.,III, McKerrow,J.H. and Wang,C.C. (1992) Steady-state kinetics of the schistosomal hypoxanthine-guanine phosphoribosyltransferase. *Biochemistry*, **31**, 806–810.

Received March 29, 1999; revised and accepted May 10, 1999